Title

Constraining bubble dynamics and mixing with dissolved gases: Implications for productivity measurements by oxygen mass balance

Journal

Journal of Marine Research, 64(1)

ISSN

0022-2402

Authors

Hamme, Roberta C
Emerson, Steven R

Publication Date

2006

Peer reviewed

Journal of Marine Research, 64, 73–95, 2006

Constraining bubble dynamics and mixing with dissolved gases: Implications for productivity measurements by oxygen mass balance

by Roberta C. Hamme[1] and Steven R. Emerson[2]

ABSTRACT

We used a dynamic mixed layer model to determine carbon export by the oxygen mass balance method from a time series of O_2/Ar, N_2/Ar and Ne measurements collected at station ALOHA near Hawaii from July 2000 to June 2001. The inert gas measurements constrain the flux of oxygen into the mixed layer from small, collapsing bubbles (injection) to be greater than or equal to the flux from larger bubbles (exchange), with mean estimates of the ratio in the range of 1–2. We also show that monthly observations of temperature and inert gases cannot constrain the rate of diapycnal mixing at this location, because of uncertainties in air-sea heat flux estimates and bubble dynamics. Organic carbon export from the mixed layer calculated from our dataset was 1.1 ± 0.5 mol C m^{-2} yr^{-1}, with most of the error deriving from uncertainties in the parameterization of diffusive gas exchange with wind speed. Our estimates of carbon export from the zone beneath the mixed layer but still in the euphotic zone ranged from 0 to 0.6 mol C m^{-2} yr^{-1} as the rate of background diapycnal mixing was increased from 0.1 to 1.0 cm^2 s^{-1}. We conclude that the oxygen mass balance method has errors of about a factor of two in areas similar to the subtropical North Pacific, with the main uncertainties deriving from mixing rates and the parameterization of diffusive gas exchange.

1. Introduction

The upper-ocean production of organic carbon and its subsequent transport to the deep ocean forces large quantities of carbon to be stored away from contact with the atmosphere. The strength of this biological pump has a direct effect on atmospheric carbon dioxide levels and climate (Siegenthaler and Sarmiento, 1993). However, its rate is difficult to directly measure and conflicting estimates abound. Some satellite-derived estimates cast the subtropics as biological deserts (Falkowski *et al.*, 1998; Laws *et al.*, 2000), while *in-situ* observations by several different methods near Hawaii suggest that the subtropics may account for up to half the global biological carbon pump (Emerson *et al.*, 1997; Sonnerup *et al.*, 1999; Benitez-Nelson *et al.*, 2001; Quay and Stutsman, 2003). As we seek to understand the

1. Scripps Institution of Oceanography, University of California San Diego, 9500 Gilman Drive, La Jolla, California, 92093-0244, U.S.A. ***email: rhamme@ucsd.edu***

2. School of Oceanography, University of Washington, Box 355351, Seattle, Washington, 98195-5351, U.S.A.

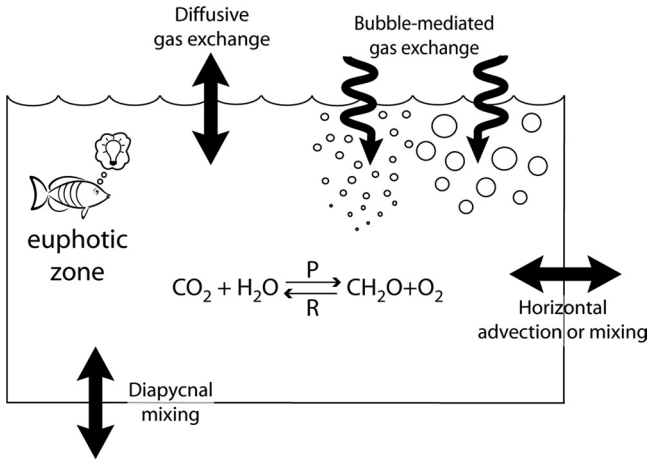

Figure 1. Schematic diagram of the important processes controlling oxygen concentrations in the upper ocean. Diffusive gas exchange refers to gas transfer across the wavy, but unbroken, air-sea interface. The reaction in the center represents photosynthesis (P) and respiration (R).

ocean carbon cycle in the face of accelerating climate change, it will be more important than ever to be able to accurately measure carbon export.

Carbon export can be determined from the net O_2 produced in the euphotic zone by photosynthesis but not subsequently consumed by community respiration (Shulenberger and Reid, 1981). Both biological and physical processes affect the cycle of oxygen in the ocean (Fig. 1). Simultaneous measurements of O_2 and inert gases have typically been used to correct for the influence of these physical processes on O_2 (Craig and Hayward, 1987; Spitzer and Jenkins, 1989; Emerson *et al.*, 1995). In this paper, we use observations of the O_2/Ar ratio in combination with a model to determine the biological component of the observed O_2 changes. Our results suggest that future use of continuous mooring or shipboard measurements of O_2 and inert gases (Emerson *et al.*, 2002; Kaiser *et al.*, 2005) will aid in determining carbon export from the mixed layer, but that additional efforts to understand mixing will be necessary to improve carbon export estimates for the whole euphotic zone.

Both bubble processes and biological production can cause the O_2 supersaturations observed in ocean mixed layers, so accounting for bubble-mediated gas exchange is important to determining productivity by this method. When breaking waves push bubbles of air beneath the surface of the ocean, hydrostatic pressure and surface tension increase the pressure inside the bubbles (Woolf and Thorpe, 1991). The added pressure increases the gradient between the gas in the bubble and the dissolved gas in the water, helping to drive gases into the water and causing supersaturation in the mixed layer. Theoretical considerations and modeling studies demonstrate that differences in the solubility and diffusion properties of gases affect their transfer to the ocean by bubbles that do not fully dissolve

(Memery and Merlivat, 1985; Fuchs *et al.*, 1987; Woolf and Thorpe, 1991; Keeling, 1993). Because Ar has very similar physical properties to O_2, it can be used to directly correct O_2 for bubble-mediated gas exchange without regard to the extent of bubble dissolution.

However, some situations call for using inert gases with less similar physical properties to correct O_2 for the effect of bubbles; for example, the recent development of methods to measure N_2 and O_2 on moorings (McNeil *et al.*, 1995; Emerson *et al.*, 2002). In this case, the degree to which the bubbles dissolve affects the magnitude of the correction and can introduce significant error. Small bubbles that completely collapse preferentially increase the concentrations of insoluble gases, while larger bubbles that transfer just a small percentage of their volume before rejoining the atmosphere preferentially increase the concentrations of gases with higher diffusion rates (Hamme and Emerson, 2002). In this paper, we use our measurements of Ne and the N_2/Ar ratio in the mixed layer to estimate the relative importance of two endmember bubble mechanisms in transferring gases to the ocean through bubbles (Fuchs *et al.*, 1987; Jenkins, 1988; Emerson *et al.*, 1997). Bubbles that completely dissolve represent one endmember, which we refer to as injection. Larger bubbles that only partially dissolve represent the other endmember, which we refer to as exchange. We additionally explore the influence of different parameterizations for the exchange mechanism, because efforts to model this mechanism have been limited by uncertainties in the size spectra of bubble plumes and the influence of turbulence, among other factors (Memery and Merlivat, 1985; Woolf and Thorpe, 1991; Keeling, 1993). A primary result of this study is constraining the injection/exchange ratio for O_2 to be greater than one, which can be used by future studies to correct O_2 for the effect of bubbles using observations of more insoluble gases like N_2.

Because O_2 has strong vertical gradients beneath the mixed layer, estimating productivity in this zone is highly sensitive to assumptions about diapycnal mixing rates. Using an annual cycle of gas observations collected from July 2000 to June 2001 at the Hawaii Ocean Time-series station ALOHA and the Price-Weller-Pinkel (PWP) dynamic mixed layer model (Price *et al.*, 1986) to provide a physical framework, we show that monthly observations of the thermal and gas cycles place no constraint on the magnitude of diapycnal mixing at this location. This is the most significant error in estimating productivity in the depth range between the base of the mixed layer and the bottom of the euphotic zone by our method. Using the same type of model to examine gas cycles in the subtropical Atlantic, Musgrave *et al.* (1988) and Spitzer and Jenkins (1989) showed that their estimates of biological O_2 production were also highly sensitive to the magnitude of turbulent mixing in the thermocline.

2. Methods

We measured depth profiles of dissolved O_2/N_2/Ar ratios and Ne concentrations in duplicate at station ALOHA (22°45'N 158°W) on 11 consecutive Hawaii Ocean Time-series cruises from July 2000 to June 2001 (HOT 117–127). Station ALOHA is located in

the central region of the North Pacific Subtropical Gyre, about 100 km north of Oahu (Karl and Lukas, 1996).

$O_2/N_2/Ar$ ratios were measured on a Finnigan MAT 251 stable isotope ratio mass spectrometer. (See Emerson *et al.* (1999) for a full description of the $O_2/N_2/Ar$ method and Hamme and Emerson (2004b) for a description of the small mass spectrometry corrections applied to the data.) The average precision of the O_2/Ar and N_2/Ar ratios in the upper 300 m (standard deviation of duplicates) was $\pm 0.07\%$. Accuracy of the mass spectrometry corrections were estimated at 0.05% for O_2/Ar and 0.01% for N_2/Ar. Suspected accuracy uncertainties on the order of $\pm 0.6\%$ for O_2 samples collected and analyzed by Winkler titration prevent very accurate estimates of Ar and N_2 concentrations from our data (Hamme, 2003). These higher error gas concentrations were used to initiate the model, but this didn't affect our results because we used the more accurate O_2/Ar and N_2/Ar ratios to constrain gas fluxes in the model.

Neon measurements were made by isotope dilution using a ^{22}Ne spike and a UTI 100C quadrupole mass spectrometer. (See Hamme and Emerson (2004a) for a full description of the Ne method.) Precision of the Ne measurements in the upper 300 m was $\pm 0.13\%$ (standard deviation of duplicates). Accuracy of the Ne saturations was estimated at $\pm 0.18\%$. Solubilities of N_2, Ar and Ne were calculated from Hamme and Emerson (2004b), and those of O_2 from García and Gordon (1992, 1993). Supersaturations in this paper are referenced to an atmospheric pressure of 1 atm including water vapor.

3. Data

During our study, the sea surface temperature (SST) at station ALOHA varied 2.5°C seasonally (Fig. 2). Vertical displacements of isotherms in the permanent thermocline on the order of 10–20 m were also observed. These features persisted over a few months, and may be related to 100–150 day oscillations in dynamic height observed at ALOHA, attributed to Rossby waves propagating through the region (Mitchum, 1996; Chiswell, 1994). To facilitate model/data comparisons, the observed profiles were normalized to the mean levels of the 21 and 14°C potential temperature isotherms, at 152 ± 17 m and 282 ± 15 m, respectively, using methods similar to those of Davis *et al.* (1981) and Price *et al.* (1978). These isotherms are below the zone affected by shortwave radiation and seasonal mixed layer dynamics. For each cruise, the observed temperature, salinity and gas profiles were stretched or compressed slightly to force the two chosen isotherms to their mean depths.

Salinity at the sea surface varied over a 0.5 (PSS) range during our study (Fig. 2), but was not correlated with the annual cycle (Bingham and Lukas, 1996). Evaporation exceeds precipitation by over one m yr^{-1} at ALOHA (da Silva *et al.*, 1994). In order to maintain the salinity balance in the mixed layer at an approximate steady state, net transport of fresher waters from the south must occur by Ekman transport driven by the trade winds (Roden, 1980). The salinity maximum at $\sim$100 m represents the core of North Pacific Central Water

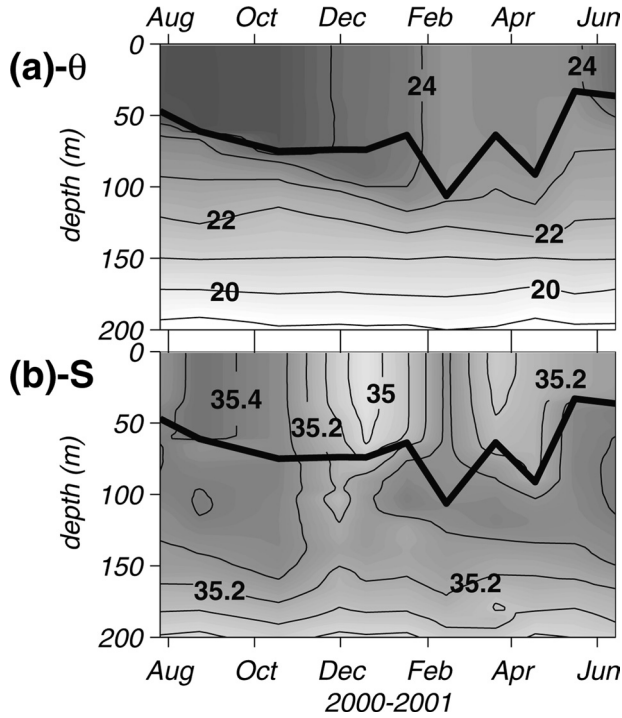

Figure 2. Contour plots for late July 2000 – June 2001 of (a) potential temperature (°C) with contour spacing of 1°C, and (b) salinity (PSS) with contour spacing of 0.1 at station ALOHA. TS data from each HOT cruise are an average in density space of 5–10 profiles. Profiles with obvious diurnal mixed layers or density inversions at the surface were excluded from the average. The average profiles were then normalized to the 21 and 14°C potential temperature isotherms as described in the text. The thick black line marks the depth of the nighttime mixed layer, defined here as the depth at which potential density exceeds the surface value by 0.1 sigma units.

(Seckel, 1968), which originates about 500 km to the north of ALOHA where evaporation exceeds precipitation by an even greater amount.

The O_2/Ar ratio is a qualitative measure of biological O_2 production. Because O_2 and Ar have similar solubilities, temperature dependencies, and molecular diffusion characteristics, the ratio with Ar to a large extent removes the effect of physical processes on O_2. We normalize the measured O_2/Ar ratio to that of the gases' equilibrium concentrations to obtain an O_2/Ar saturation ratio,

$$\Delta O_2/Ar = ((O_2/Ar)/(O_{2S}/Ar_S) - 1) * 100 \quad (1)$$

where O_{2S} is the equilibrium concentration of O_2 etc.… The upper 100 m of the water column at ALOHA was supersaturated in $\Delta O_2/Ar$ for most of the year

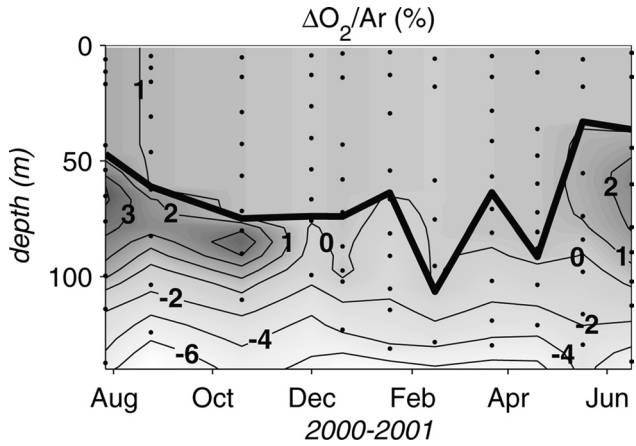

Figure 3. Contour plot of the O_2/Ar saturation ratio (in percent) for late July 2000 – June 2001 at ALOHA. Contour spacing is 1% above zero, and 2% below. The thick black line marks the depth of the nighttime mixed layer. Dots mark the sampling times and depths.

(Figs. 3 and 4). Typical of subtropical gyres during the summer (Shulenberger and Reid, 1981; Jenkins and Goldman, 1985; Emerson *et al.*, 1995), a subsurface oxygen maximum began to develop in late spring and lasted through the fall, with $\Delta O_2/Ar$ exceeding 3% in some months. Negative $\Delta O_2/Ar$ values and a steep gradient beneath about 100 m indicate the progressively greater dominance of respiration at depth.

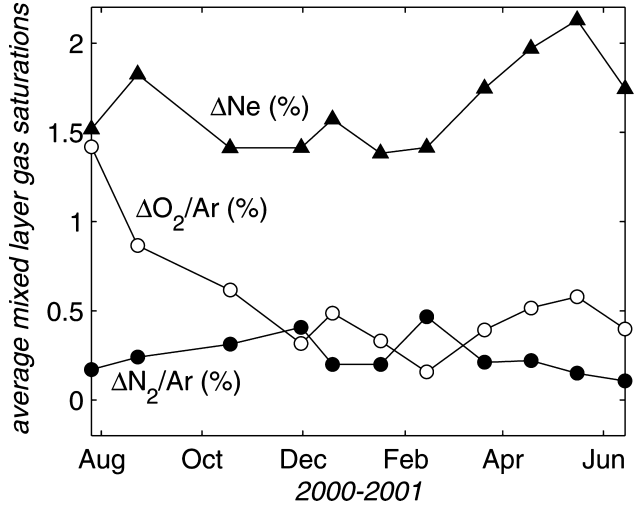

Figure 4. Average Ne supersaturations and O_2/Ar and N_2/Ar saturation ratios in the mixed layer (in %) for late July 2000 – June 2001 at ALOHA. Ne supersaturations are not corrected for atmospheric pressure, which was 1.005 atm on average at ALOHA for this time period.

The N_2/Ar ratio in the mixed layer is primarily driven by bubble processes (Schudlich and Emerson, 1996), because N_2 is about half as soluble as Ar. Here again, we normalize the measured ratio to the equilibrium ratio to obtain $\Delta N_2/Ar$. Higher $\Delta N_2/Ar$ values observed during the winter may be driven by storms (Fig. 4). Neon saturations are forced by both bubble processes and temperature change. The heating and cooling cycle of the mixed layer caused Ne saturations to be generally higher during spring/summer relative to winter. However, measured Ne supersaturations were always about a percent greater than atmospheric pressure, indicating the dominance of bubble fluxes over cooling even in the winter. We will use both $\Delta N_2/Ar$ and ΔNe to constrain bubble processes within the model.

4. Upper ocean model description

Previous calculations of biological O_2 production from gas measurements at ALOHA were based on a 3-box model (Emerson *et al.*, 1995, 1997). Here, we use a dynamic mixed-layer model that combines gas cycling with the Price *et al.* (1986) physical model (PWP). This model allows a more realistic exploration of the effects of mixing and temperature change on gas saturations.

Briefly, the model's initial conditions were taken from the average temperature, salinity and gas profiles observed in July 2000. At each one hour time step, heat and momentum fluxes were added to and removed from the water column based on meteorological data. Mixing was determined by meeting the three stability criteria of Price *et al.* (1986) over which a constant eddy diffusivity was also imposed. The mixed layer in this type of model is homogeneous. We divided gas exchange into separate diffusive and bubble-mediated processes with diffusive gas exchange parameterized from wind speed. A model inversion was used to determine the bubble fluxes necessary to reproduce the observed ΔNe and $\Delta N_2/Ar$ in the mixed layer and to determine the biologically-driven O_2 fluxes necessary to reproduce the observed $\Delta O_2/Ar$ profiles.

a. Meteorological inputs

Estimates of downward solar radiation flux and cloud cover for the 2000–2001 time period at ALOHA were obtained on a six-hourly timescale from the National Centers for Environmental Prediction (NCEP) Reanalysis dataset (Kalnay and Coauthors, 1996). During 1991–1993, NCEP solar radiation compared well with estimates from the International Satellite Cloud Climatology Program (ISCCP) (Bishop *et al.*, 1997) at this location. We applied a fixed 6% albedo correction (Payne, 1972). Light attenuation into the ocean was modeled using a double exponential as in Paulson and Simpson (1977).

$$I(z)/I(0) = 0.49e^{-0.040z} + 0.51e^{-z} \tag{2}$$

where $I(z)$ is the irradiance at depth z (positive downward), the first term on the right side of the equation represents the penetration of photosynthetically active radiation (PAR)

(Baker and Frouin, 1987; Letelier *et al.*, 2004), and the last term the penetration of longer wavelengths (Paulson and Simpson, 1977).

Hourly wind speed, wind direction, air temperature, and sea level pressure observations were obtained from National Data Buoy Center (NDBC) meteorological buoy 51001, located at 23.4N, 162.3W, about 450 km mostly to the west of station ALOHA. Latent and sensible heat fluxes were calculated using the TOGA COARE algorithms (Fairall *et al.*, 1996) from buoy observations, model SSTs, and a tunable relative humidity parameter. Basing heat fluxes on model SSTs helped prevent model drift. Outgoing longwave radiation was calculated using the Clark *et al.* (1974) algorithm from buoy air temperatures, NCEP cloud cover, model SSTs, and tuned relative humidity (Josey *et al.*, 1997). Heat loss from the ocean creates a thin cool skin at the surface, which affects gas exchange by altering gas solubilities (Robertson and Watson, 1992; Asher and Wanninkhof, 1998b). This cool skin temperature, as calculated by the TOGA COARE algorithm (Fairall *et al.*, 1996), was 0.21 ± 0.04°C less than the bulk temperature and displayed no annual cycle.

Humidity was treated as a tunable parameter because high quality estimates could not be obtained for this location and time period. During 1997–1999, NCEP humidities were on average 15% higher than those measured at the HALE ALOHA mooring. We optimized the average humidity for each time period between cruise observations so that the model reproduced observed SSTs. Those tuned relative humidity values were 71 ± 6%, identical to the mean and standard deviation observed at the HALE-ALOHA mooring for 1997–1999. Our humidity tuning procedure eliminated the possibility of independently calculating the thermal cycle. However, some form of heat flux tuning is usually necessary in one-dimensional models that operate over long time periods (Musgrave *et al.*, 1988; Large *et al.*, 1994; Kantha and Clayson, 1996; Doney, 1996), both because of errors inherent in the estimation of individual heat fluxes (on the order of 10 W m^{-2} (Fairall *et al.*, 1996)) and because lateral heat fluxes are not taken into account.

b. Physical model

In this model, solar radiation acted to stratify the water column while the combination of latent, sensible and outgoing longwave heat fluxes always acted to cool the top layer. After addition and removal of heat and momentum at each time step, the mixed layer depth was determined by satisfying convective and sheer stability parameters. An additional shear flow stability criteria, controlled by a gradient Richardson number, was applied to smooth the transition zone at the base of the mixed layer. These three mixing criteria were implemented exactly as described in Price *et al.* (1986). Salinity in the model was relaxed to the observations on a timescale of 30 days, because advection plays a substantial role in the salinity budget at ALOHA. Beyond this salinity adjustment, the effects of lateral or vertical advection were not included in the model.

A constant background eddy diffusivity was also applied over the entire water column, with tracer concentrations at the base of the modeled water column (300 m) held constant.

We tested eddy diffusivities (K_z) of 0.1–1.0 $cm^2\ s^{-1}$ to explore the impact on our conclusions about gas cycling. Background values of eddy diffusivity in the thermocline are generally near 0.1 $cm^2\ s^{-1}$, though they may be 1–2 orders of magnitude higher just below the mixed layer (Gregg, 1989; Brainerd and Gregg, 1993; Gregg, 1998). At ALOHA, estimates of eddy diffusivity in the thermocline (200–500 m) are near these background levels (Finnigan *et al.*, 2002). However, both box models used at ALOHA (Emerson *et al.*, 1995; Quay and Stutsman, 2003) and PWP models used at the Bermuda Atlantic Time-series Study (BATS) (Musgrave *et al.*, 1988; Spitzer and Jenkins, 1989) employ high eddy diffusivities (0.75–1.5 $cm^2\ s^{-1}$) to explain observed gas data.

c. Gas model

Oxygen, N_2, Ar and Ne were incorporated into the model and subjected to the same mixing processes as temperature and velocity. The model's initial gas profiles were set to the profiles measured in July 2000. Air-sea gas exchange altered gas concentrations in the mixed layer, and was modeled as the sum of a diffusive component representing transfer across the wavy but unbroken air-sea interface, and a bubble-mediated component. To determine the sensitivity of our results to uncertainties in diffusive gas exchange, we tested the wind speed parameterizations of Liss and Merlivat (1986), Nightingale *et al.* (2000), and Wanninkhof (1992), with a Schmidt number dependence of −0.5 (Jähne *et al.*, 1987).

Bubble-mediated gas exchange was parameterized as a combination of fluxes from two different bubble mechanisms: injection (V_{inj}), which refers to collapsing bubbles, and exchange (V_{ex}), which refers to partially dissolving bubbles (Fuchs *et al.*, 1987; Jenkins, 1988; Schudlich and Emerson, 1996; Hamme and Emerson, 2002).

$$B_C = \left(V_{inj} + V_{ex} D_C^x \alpha_C^y\right) \chi_C \tag{3}$$

where D_C is the diffusion coefficient, α_C the Bunsen solubility coefficient, and χ_C the atmospheric mole fraction of gas C. The best dependence of the exchange bubble mechanism on the diffusion and solubility properties of the gases is unclear, so we tested the sensitivity of our results to three different formulations. The first relationship is based on the theoretical flux from bubbles that spend so little time submerged that the ratio of gases inside the bubble does not change significantly (Hamme and Emerson, 2002). The flux of gases from this bubble type is proportional to the solubility of each gas and the square root of its diffusion coefficient ($x = 0.5$, $y = 1$). The second relationship, proposed by Jenkins (1988), is similar but assumes that the bubbles are dirty ($x = 0.67$, $y = 1$). The third relationship, developed by Keeling (1993) based on a model of bubble processes, suggests the dependence should be $x = 0.35$ and $y = 0.7$.

Whitecaps have been shown to scale approximately with the cube of the wind speed (Asher and Wanninkhof, 1998a), though many simpler gas models ignore the dependence of bubble fluxes on wind speed (Emerson *et al.*, 1995). We tested scaling bubble-mediated gas exchange in three different ways: (1) constant bubble fluxes; (2) bubble fluxes proportional

to wind speed; and (3) bubble fluxes proportional to wind speed cubed. For cases two and three, bubble fluxes were set to zero for wind speeds below 2.27 m s^{-1} (Monahan and Torgersen, 1991).

For each time period between cruises, a minimizing optimization scheme was used to determine the fluxes from the two bubble mechanisms, V_{inj} and V_{ex}, that were best able to reproduce the mean mixed layer ΔNe and $\Delta N_2/Ar$ observed at the end of the time period. This procedure was able to reduce model/data differences in these tracers to arbitrarily low values. We found that $\Delta N_2/Ar$ is only sensitive to the injection mechanism, while fluxes from both bubble mechanisms affect ΔNe, so that $\Delta N_2/Ar$ and ΔNe are linearly independent in determining the fluxes from our different bubble mechanisms (see Appendix).

Profiles of net biological O_2 production were determined using an iterative process. During each time period between observations, an abiotic model run provided an initial productivity guess, which was refined by adjusting the productivity profile until the model $\Delta O_2/Ar$ matched observed profiles within 0.05% at every depth. For a couple of months when the model mixed layer depth was slightly greater than observed, this procedure would have produced spuriously large biological productions if the model had tried to reproduce observed subsurface O_2 maximums that were within the model's mixed layer. In these cases, the entire model mixed layer was forced to reproduce the average $\Delta O_2/Ar$ in the observed mixed layer rather than trying to match the details of the profile exactly in this region.

5. Results and discussion

The model approximately reproduces the seasonal cycle of temperature and mixing at station ALOHA (Fig. 5). Because humidities were tuned, model SSTs exactly matched the observations, which was important to accurately calculate gas solubilities and gas exchange rates. Changes in the heat content of the model water column tracked the observations, so we made no advective heat adjustments. Autumnal deepening of the mixed layer was somewhat slower in the model, and was not improved by altering model parameterizations or initial conditions within reasonable limits. Inadequate vertical mixing in the PWP model has been noted in other model/data comparisons (Large and Crawford, 1995; Kantha and Clayson, 1996; Large *et al.*, 1994). An advective cooling event at 50–100 m during the late spring is also not well simulated by the model. However, these model/data inconsistencies do not hamper our investigation of bubble-mediated gas exchange, mixing in the thermocline, and biological productivity.

a. Bubble fluxes

Using ΔNe and $\Delta N_2/Ar$ measurements to constrain modeled bubble-mediated gas exchange, we found that the fluxes of O_2 into the mixed layer through the injection and exchange bubble mechanisms were about 1.4 and 0.9 mol O_2 m^{-2} yr^{-1}, respectively (Fig. 6). These bubble fluxes were comparable in magnitude to diffusive gas exchange at about 3.5 and biological production at about 2 mol O_2 m^{-2} yr^{-1}.

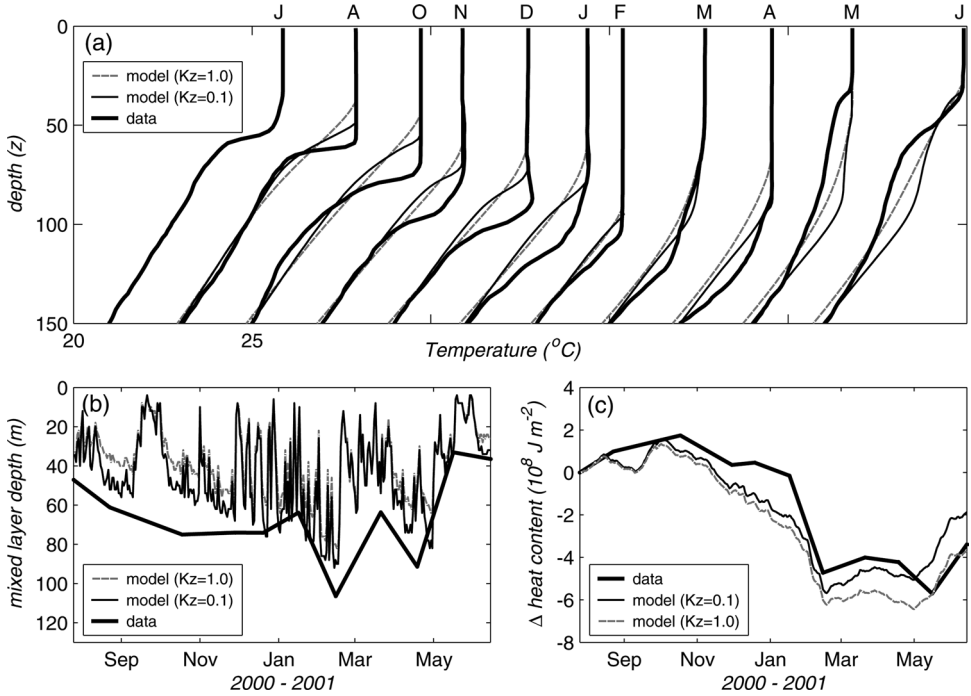

Figure 5. Data/Model comparisons for two model runs with eddy diffusivities (K_z) of 0.1 and 1.0 $cm^2\ s^{-1}$ (a) Observed and modeled temperature profiles. Each profile is offset by 2°C from the one before. Letters at the top indicate the month of the observation, beginning in July 2000. (b) Observed and modeled mixed layer depths (m). Model mixed layers are the deepest calculated for each diurnal cycle. (c) Observed and modeled cumulative changes in the heat content of the upper 200 m of the water column (10^8 J m^{-2}).

The model-derived injection/exchange ratio was robust to the choice of diffusive gas exchange parameterizations, dependencies of bubble fluxes on wind speed, and eddy diffusivities (Fig. 6). Increasing the diffusive flux of gases out of the mixed layer, by moving from the Liss and Merlivat (1986) parameterization through Nightingale *et al.* (2000) to Wanninkhof (1992), also increased bubble fluxes into the mixed layer in order for the model to reproduce the observations. This whole range in diffusive gas exchange parameterizations resulted in only a 1.1-1.4 range in the injection/exchange ratio. Allowing the bubble fluxes to depend on wind speed resulted in greater temporal variability in the bubble fluxes, but had little effect on the annually integrated fluxes or on the injection/exchange ratio. Finally, the overall impact of eddy diffusivity on model bubble fluxes was small, with an increase of almost 1 $cm^2\ s^{-1}$ in diffusivity only raising the injection/exchange ratio from 1.3 to 1.9. Mixing had less impact on the derived bubble fluxes in this model as compared with Emerson *et al.* (1995), because the depth gradients of ΔNe and $\Delta N_2/Ar$ are much weaker than the gradients in Ar and N_2 concentrations.

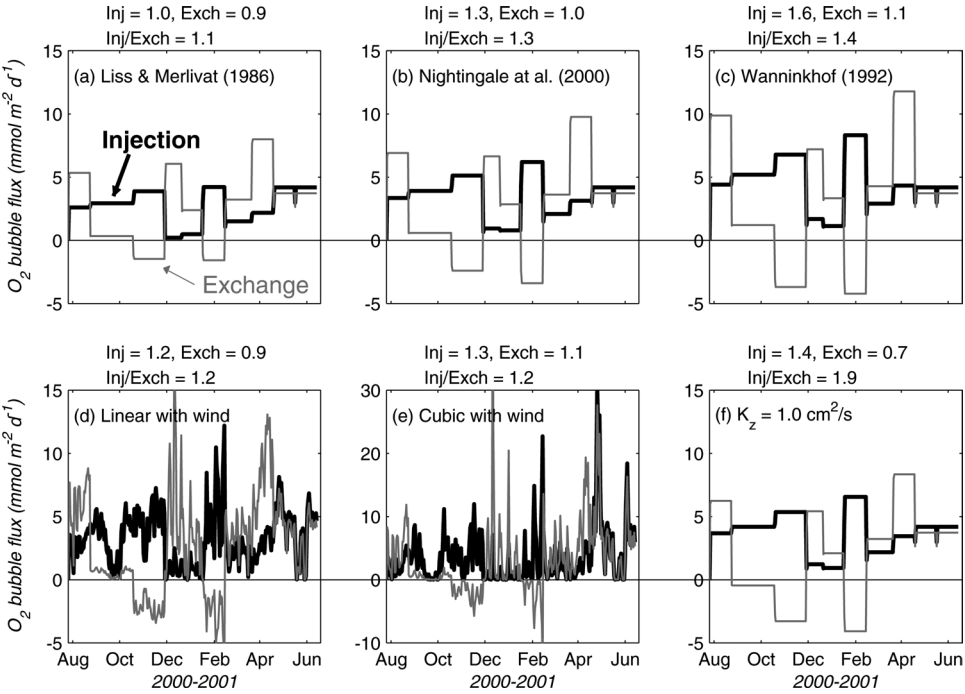

Figure 6. Modeled daily fluxes of O_2 through the injection and exchange bubble mechanisms (mmol O_2 m^{-2} d^{-1}). The integrated flux for the year through injection (Inj) and exchange (Exch) (in mol O_2 m^{-2} yr^{-1}) and the injection/exchange ratio (Inj/Exch) for each parameter combination is given above the graphs. Unless otherwise noted, the model runs use the Nightingale *et al.* (2000) gas exchange parameterization, have bubble fluxes independent of wind speed, and an eddy diffusivity (K_z) of 0.1 cm^2 s^{-1}. The Hamme and Emerson (2002) parameterization is used for the exchange bubble mechanism in all cases. (a) Liss and Merlivat (1986) gas exchange parameterization. Each horizontal line segment shows the flux during a period between field observations. (b) All parameters standard. (c) Wanninkhof (1992) gas exchange parameterization. (d) Bubble fluxes are linearly dependent on wind speed. (e) Bubble fluxes are related to the cube of the wind speed. Note that the scale on the y-axis is expanded for this graph. (f) Eddy diffusivity of 1.0 cm^2 s^{-1}.

We found that the choice of solubility and diffusion coefficient dependence for the exchange bubble mechanism had no effect on the model's predictions of the total flux of O_2 into the mixed layer through bubbles. Using the Keeling (1993) parameterization ($V_{ex} D_C^{0.35} \alpha_C^{0.7} \chi_C$) in place of the Hamme and Emerson (2002) parameterization ($V_{ex} D_C^{0.5} \alpha_C \chi_C$) did result in a shift from injection to exchange, but the combined O_2 flux from both mechanisms was unchanged. The Jenkins (1988) parameterization ($V_{ex} D_C^{0.67} \alpha_C \chi_C$) yielded extremely similar results to the Hamme and Emerson (2002) parameterization, because all our tracers have similar diffusion coefficients.

The annually integrated values for the injection and exchange bubble fluxes from our model were robust (Table 1), as shown by a Monte Carlo analysis (Press *et al.*, 1995). We

Table 1. Comparison of bubble-mediated O_2 fluxes (in mol O_2 m^{-2} yr^{-1}) into the euphotic zone for model runs with eddy diffusivities (K_z) of 0.1 and 1.0 cm^2 s^{-1} and alternative parameterizations of the exchange mechanism. Results are based on 180 Monte Carlo runs for each case.

	$K_z = 0.1$	$K_z = 1.0$
Hamme and Emerson (2002) exchange mechanism parameterization ($V_{ex} D_C^{0.5} \alpha_C \chi_C$)		
Injection	1.3 ± 0.4	1.4 ± 0.3
Exchange	1.0 ± 0.7	0.7 ± 0.7
Injection/Exchange ratio	$1.1 + 2.0 - 0.4$	$1.9 + 40 - 1.0$
Keeling (1993) exchange mechanism parameterization ($V_{ex} D_C^{0.35} \alpha_C^{0.7} \chi_C$)		
Injection	1.0 ± 0.4	1.1 ± 0.5
Exchange	1.3 ± 1.0	1.0 ± 1.1
Injection/Exchange ratio	$0.6 + 2.0 - 0.3$	$0.8 + \infty - 0.4$

ran the model many times, applying random deviations with Gaussian distributions to the data or parameterizations controlling bubble fluxes for each run, with the following standard deviations: mixed layer ΔNe $\pm$0.20%, mixed layer $\Delta N_2/Ar$ $\pm$0.040%, and the diffusive gas exchange parameterization of Nightingale *et al.* (2000) $\pm$30%. The randomly chosen deviation was applied to the entire year's data, not to each individual month. Inert gas errors were estimated from errors in precision (standard deviation of the mean) and accuracy (possible systematic errors), whereas the range in the diffusive gas exchange coefficient was chosen to approximately encompass the parameterizations of Liss and Merlivat (1986) and Wanninkhof (1992). Although errors in both the injection and exchange fluxes appeared normally distributed, error in the ratio of injection to exchange had a skewed distribution. We give the mean injection/exchange value determined from each set of Monte Carlo analyses along with the asymmetric errors encompassing 68% of values (Table 1).

b. Diapycnal mixing

In this section, we show that monthly measurements of temperature and gases can not be used to determine the rate of background diapycnal mixing at station ALOHA. In the next section, we show that these uncertainties in mixing add significant error to the determination of biological O_2 production beneath the mixed layer.

Increasing the eddy diffusivity in the model from 0.1 to 1.0 cm^2 s^{-1} resulted in a shallower mixed layer and a more gradual temperature gradient beneath the mixed layer (Fig. 5). However, the two model runs with different diffusivities were more similar to each other than either model run was to the observations. Also, because the model is somewhat deficient in representing mixing near the base of the mixed layer, data / model comparisons of the water column directly beneath the mixed layer are an inappropriate tool to constrain background eddy diffusivity over the whole water column.

Surface heat fluxes estimated from meteorological measurements or climate products like NCEP were not accurate enough to constrain eddy diffusivity at ALOHA. Implementations

Table 2. Comparison of the annual average heat fluxes (in W m^{-2}) into the euphotic zone necessary for the model to reproduce observed SSTs when different eddy diffusivities (K_z in cm^2 s^{-1}) were used.

	$K_z = 0.1$	$K_z = 1.0$
Net solar radiation	235	235
Outgoing longwave	−62	−60
Sensible	−3	−3
Latent	−167	−156
Mixing	−2	−17
Storage	2	−1

of the PWP model near Bermuda used data / model comparisons of SSTs and subsurface heating to constrain eddy diffusivities to ∼1 cm^2 s^{-1} (Musgrave *et al.*, 1988; Spitzer and Jenkins, 1989). At ALOHA, in order to continue to reproduce observed SSTs while raising the eddy diffusivity from 0.1 to 1.0 cm^2 s^{-1}, it was only necessary to lower the surface heat flux by 11 W m^{-2} (by raising humidity 2%) to compensate for the cooling of the water column by increased mixing of cold water up from below (Table 2). This order 10 W m^{-2} difference between the two mixing cases, a difference in cumulative heat flux of $3*10^8$ J m^{-2} yr^{-1}, is well within the uncertainties of NCEP heat fluxes (Smith *et al.*, 2001), so we have no independent means of preferring one mixing scenario over the other. Indeed, cumulative heat fluxes for this area from the NCEP Reanalysis dataset fell between our model derived heat fluxes for the low and high diffusivity cases (Fig. 7). Additionally, Ekman transport from the south and geostrophic transport from the north-east add further error to the heat budgets at ALOHA, but were not considered in this one-dimensional model. While we have only investigated constraining eddy diffusivity at station ALOHA,

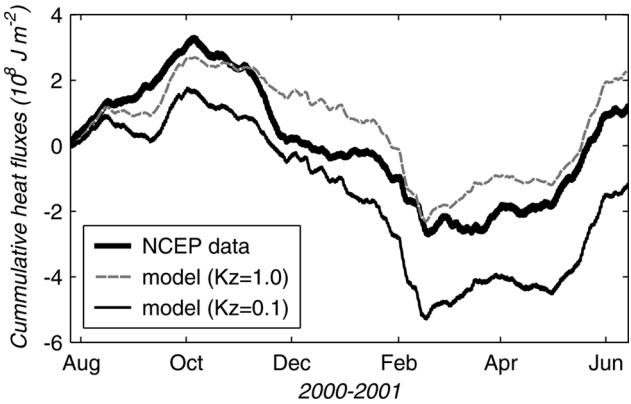

Figure 7. Cumulative air-sea heat fluxes at station ALOHA from the NCEP Reanalysis dataset compared to model runs with eddy diffusivities (K_z) of 0.1 and 1.0 cm^2 s^{-1}. Heat fluxes are the sum of net shortwave radiation, outgoing longwave radiation, sensible and latent heat fluxes.

Table 3. Comparison of annual Ar fluxes (in mmol Ar m^{-2} yr^{-1}) into the euphotic zone for model runs with eddy diffusivities (K_z) of 0.1 and 1.0 cm^2 s^{-1}. Both runs use the Nightingale *et al.* (2000) gas exchange parameterization, and assume that bubble fluxes are independent of wind speed. The last column is the difference between the two model runs.

	$K_z = 0.1$	$K_z = 1.0$	Change
Mixing	1.4	20.7	19.3
Gas exchange	−83.9	−88.3	−4.4
Bubble injection	45.1	48.3	3.2
Bubble exchange	50.7	37.4	−13.3
Storage	13.3	18.1	4.8

our conclusions demonstrate the importance of considering the errors in heat flux estimates like NCEP to attempts to estimate diapycnal mixing at any location.

Using N_2 and Ar data collected at ALOHA in previous years, Emerson *et al.* (1995, 1997) developed a 3-box model to calculate both the rate of diapycnal mixing and the gas flux through bubbles, assuming a fixed injection/exchange ratio for the bubble flux. Applying this 3-box model to our 2000–01 N_2 and Ar data suggested that the gases could constrain eddy diffusivity within ± 0.6 cm^2 s^{-1} for a given injection/exchange ratio. This error estimate was based on a Monte Carlo analysis with coinciding errors of $\pm 0.2\%$ in the N_2 and Ar data (Emerson *et al.*, 1995). We see now that assuming a single injection/exchange ratio in the 3-box model provided an inappropriate extra constraint for the calculation of diapycnal mixing by that model. We tested removing this assumption by constructing a similar 3-box model that incorporated Ne data to solve for the injection/exchange ratio while still assuming the same errors in just the N_2 and Ar data. This new box model suggested that eddy diffusivity could only be constrained within ± 1.6 cm^2 s^{-1}, nearly three times greater than when the injection/exchange ratio was held constant.

In the PWP model described in this paper, increasing eddy diffusivity from 0.1 to 1.0 cm^2 s^{-1} resulted in an order of magnitude increase in the delivery of Ar, for example, to the euphotic zone (Table 3). Because this model dynamically solves for bubble fluxes, the increased flux from mixing was compensated for by smaller bubble fluxes and larger losses by diffusive gas exchange. The total effect in the mixed layer amounted to only a 0.02% increase in ΔAr from the low to high mixing cases, far less than current measurement errors (Emerson *et al.*, 1999). Increasing eddy diffusivity had a larger impact on ΔAr beneath the mixed layer where a subsurface summertime maximum forms due to heating by local solar radiation. However, again because the way mixing is treated in this region below the mixed layer is more a function of the chosen model's dynamics than background eddy diffusivity, we did not use differences in the subsurface gas saturations to attempt to constrain diapycnal mixing for the deeper water column. Thus, we have shown that inert gas measurements can not provide a constraint over diapycnal mixing at ALOHA, either in a simple box model or in a more complicated dynamic mixed layer model.

Table 4. Comparison of O_2 fluxes (in mol O_2 m^{-2} yr^{-1}) into the euphotic zone for model runs with eddy diffusivities (K_z) of 0.1 and 1.0 cm^2 s^{-1}. Means and standard deviations are based on 180 Monte Carlo runs for each case. Biological production is listed for the total euphotic zone as well as components from just the mixed layer and from the layer from the base of the mixed layer to the base of the euphotic zone (defined by the 1% light level at 114 m (Letelier *et al.*, 2004)).

	$K_z = 0.1$	$K_z = 1.0$
Total biological production	1.5 ± 0.8	2.5 ± 0.7
…in mixed layer	1.5 ± 0.8	1.6 ± 0.7
…from mixed layer base to base of euphotic zone	-0.02 ± 0.01	0.90 ± 0.01
Diffusive gas exchange	-3.6 ± 1.5	-3.9 ± 1.3
Mixing	-0.06	-0.51
Bubble-mediated gas exchange	2.3 ± 0.8	2.1 ± 0.8
Storage	0.11 ± 0.04	0.22 ± 0.05

c. Biological oxygen production

The degree to which diapycnal mixing can be constrained has an important effect over the determination of carbon export from oxygen measurements. Net biological O_2 production increased by 70% when eddy diffusivity was increased from 0.1 to 1.0 cm^2 s^{-1} in our model, with all of the increase occurring below the mixed layer (Table 4). Increased mixing moves O_2 along the steep gradients from the euphotic zone down to the deeper ocean and up to the mixed layer (Fig. 3), forcing the model to solve for greater biological production to replace this mixing deficit. In contrast, our determination of net biological O_2 production in the mixed layer was not significantly affected by the rate of diapycnal mixing. Biological production in the mixed layer was about 50% higher from March through October.

Uncertainty in the diffusive gas exchange parameterization was the most important error in determining biological production in the mixed layer, while the uncertainty in diapycnal mixing was most important to the area below the mixed layer. Errors in the O_2 budget terms were also determined from our Monte Carlo analysis (Table 4). We applied an error of $\pm 0.068\%$ to $\Delta O_2/Ar$ along with $\pm 30\%$ to the Nightingale *et al.* (2000) diffusive gas exchange parameterization, $\pm 0.20\%$ to ΔNe, and $\pm 0.040\%$ to $\Delta N_2/Ar$. Some errors resulted in fluxes that offset each other. For example, when the diffusive gas exchange rate was increased, bubble fluxes and biological production also increased to compensate, but the change in O_2 between the beginning and end of the model run, the storage term, was little altered. A sense of the error imparted by the uncertainty in diapycnal mixing can be gained from the difference between the two sets of Monte Carlo runs for eddy diffusivities of 0.1 and 1.0 cm^2 s^{-1}.

The contribution of each individual uncertainty was determined from separate Monte Carlo analyses in which just one input was allowed to vary. The error in diffusive gas exchange contributed ± 0.6 mol O_2 m^{-2} yr^{-1} to the total error in biological productivity, while errors in $\Delta O_2/Ar$, ΔNe and $\Delta N_2/Ar$ contributed ± 0.2, ± 0.1, and ± 0.04 mol O_2 m^{-2} yr^{-1}, respectively. The errors in ΔNe and $\Delta N_2/Ar$, the parameters used to

Table 5. Comparison of the average annual net organic carbon export derived from this model with previous estimates at station ALOHA (mol C m^{-2} yr^{-1}).

Source of data	Organic carbon export
This study with $K_z = 0.1$ cm^2 s^{-1}: O_2 mass balance	1.1 ± 0.5
This study with $K_z = 1.0$ cm^2 s^{-1}: O_2 mass balance	1.8 ± 0.5
Christian (2005): Ecosystem modeling	0.6 – 0.8
Quay and Stutsman (2003): DIC mass balance	2.7 ± 1.3
Benitez-Nelson *et al.* (2001): ^{234}Th export	2.4 ± 0.9
Emerson *et al.* (1997): O_2 mass balance	2.7 ± 1.7

Carbon export was calculated from net biological O_2 production using a production quotient of 1.4 (Anderson, 1995).

tune the bubble fluxes, had a negligible impact because $\Delta O_2/Ar$ data was used to constrain productivity. Oxygen and Ar have almost the same solubilities and diffusivities, so a wide range of bubble fluxes result in widely ranging O_2 and Ar concentrations but similar $\Delta O_2/Ar$ ratios in the mixed layer. If biological O_2 production had been calculated from O_2 concentrations or $\Delta O_2/N_2$ ratios, the errors in determining bubble fluxes would have had a much larger effect.

Previous observations of organic carbon export at ALOHA just barely overlap with our estimate using the lower eddy diffusivity of 0.1 cm^2 s^{-1}, which we consider a lower bound for carbon export from our method (Table 5). Using the higher eddy diffusivity, our estimate was still on the low side but more comfortably within the uncertainties of these previous observations, most of which also employ high diffusivities. In contrast, the ecosystem-model-derived estimate of Christian (2005) was on the low side of our lower-bound carbon export estimate. Station ALOHA exhibits significant interannual variability (Fujieki *et al.*, 2004), and this variability may account for some of the differences between our estimates, which are relevant only for summer 2000 through summer 2001, and those of previous investigators.

6. Conclusions

Using ΔNe and $\Delta N_2/Ar$ ratios in combination with the Price *et al.* (1986) mixed layer model, we constrained the flux of O_2 from bubbles through the injection mechanism to be greater than or equal to the flux through the exchange mechanism. This ratio was robust to uncertainties in the relationship between bubble fluxes and wind speed, the parameterization of diffusive gas exchange, and the rate of diapycnal mixing. Determining productivity from O_2/Ar ratios removes the need to quantify bubble processes, but this measurement can not yet be made from moorings or floats, while continuous measurements of O_2 and N_2 can (Emerson *et al.*, 2002). The difference in solubility between O_2 and N_2 makes the correction for bubble processes more important. The injection/exchange ratio determined from this paper can be applied to continuous O_2 and N_2 measurements to improve the bubble correction, though more information on spatial and temporal variations in this ratio will increase confidence in its application.

The large uncertainties in heat flux estimates as well as the effects of horizontal advection make it impossible to determine diapycnal mixing rates within a factor of ten from monthly observations of temperature at ALOHA. We also found that gas measurements could not constrain diffusivity in our model, and that removing an assumption about the injection/exchange ratio from the box model of Emerson *et al.* (1995, 1997) rendered it similarly unable to constrain mixing.

Uncertainty in diapycnal mixing has little effect on determinations of carbon export in the mixed layer by the oxygen mass balance method, but a significant effect for determinations from the entire euphotic zone. Because the productivity measurement in the mixed layer is mainly sensitive to gas exchange across the air-sea interface, capturing spatial and temporal variability in air-sea gradients by continuous measurement of dissolved O_2/Ar from ships (Kaiser *et al.*, 2005) or dissolved O_2 and N_2 from moorings (Emerson *et al.*, 2002) should result in improved export estimates for this portion of the water column. However, until the physics of mixing in the tens of meters below the base of the mixed layer are better understood, increased sampling may not yield improvements in estimates for the whole euphotic zone. Ideally, measurements of O_2 and inert gases will be combined with a field program specifically designed to determine shallow diapycnal mixing rates.

Acknowledgments. We wish to thank Charles Stump for his unstinting efforts in sample collection and analysis for this project, and David Wilbur for aid in defining the mass spectrometric corrections. The HOT scientists and the crew of the R/V *Ka'imikai-O-Kanaloa* were very helpful in accommodating our sample collection and data needs. Matthew Alford, William Asher, James Christian, Eric D'Asaro, Jody Klymak, Eric Kunze, Carol Ladd, Ricardo Letelier, Jonathan Nash, and Yvette Spitz are all thanked for their advice on aspects of the model. This manuscript has benefited from the critical comments of Paul Quay, Allan Devol, Eric D'Asaro and two anonymous reviewers. We thank NSF (OCE-9617487 and OCE-9819181) for their support of this project, and NASA (ESS/99-0000-0022) and the Comer Climate Change Foundation for support of Roberta. Finally, we gratefully acknowledge meteorological data and computer code from other sources: NCEP Reanalysis data was provided by the NOAA-CIRES Climate Diagnostics Center, Boulder, Colorado, USA, (http://www.cdc.noaa.gov/), buoy data by the National Data Buoy Center (http://www.ndbc.noaa.gov/), ISCCP solar radiation data by James K. B. Bishop at the Lawrence Berkeley National Laboratory (http://www.ocean.lbl.gov/seawifs.html), and meteorological data from the HALE-ALOHA mooring data by Pierre Flament at the University of Hawaii (http://hahana.soest.hawaii.edu/hot/hale-aloha/ha.html). A MatLab version of the PWP model with gas tracers was developed by William Jenkins (http://w3eos.whoi.edu/12.747/notes/lect19-20/l19s03c.html), and a Fortran version obtained from Jim Price (http://www.whoi.edu/science/PO/people/jprice/PWP/welcome.html).

APPENDIX

Constraint of bubble mechanisms by $\Delta N_2/Ar$ and ΔNe

Because the exchange bubble mechanism, especially the Hamme and Emerson (2002) and Jenkins (1988) parameterizations, transfers N_2 and Ar to the ocean in almost the same ratio as their solubility concentrations, N_{2S}/Ar_S, the flux from this class of bubbles has

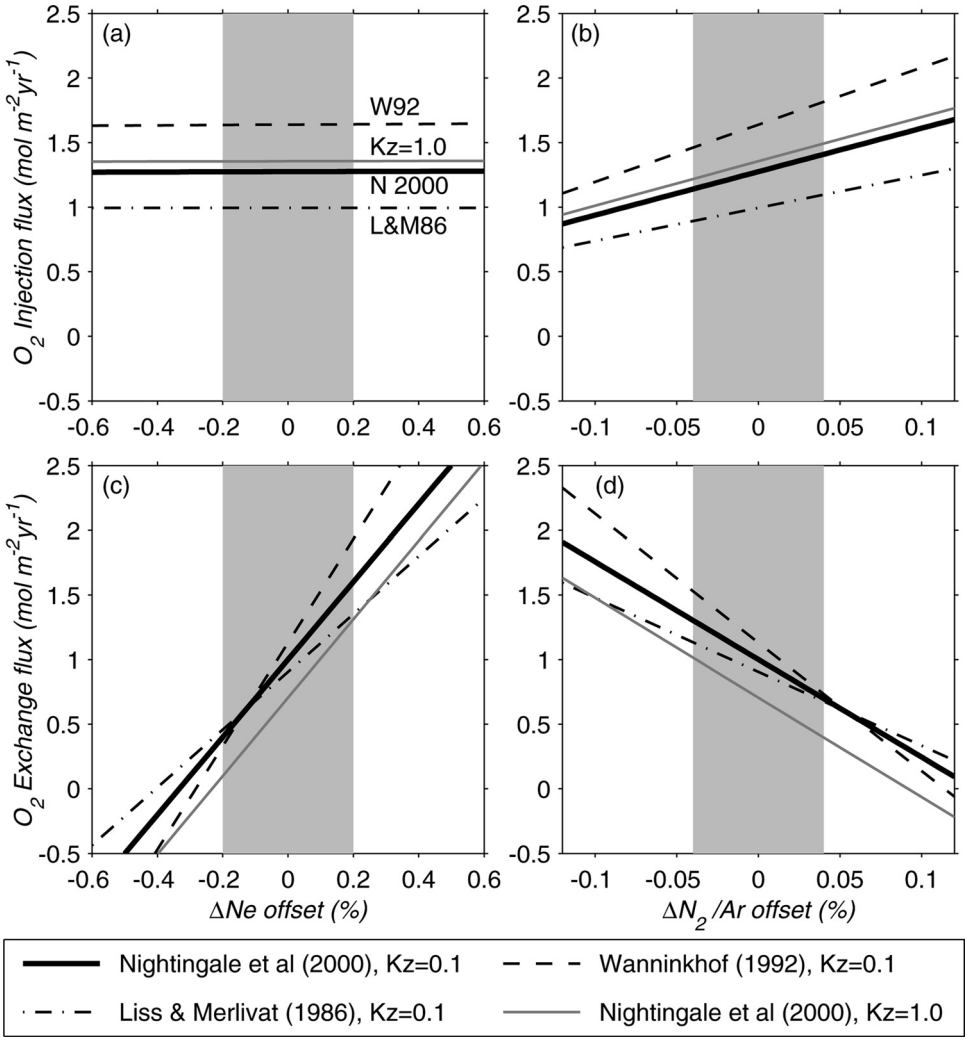

Figure A1. The effect of errors in the inert gas data on model-derived bubble fluxes of O_2 into the mixed layer through the injection mechanism (a-b) and the exchange mechanism (c-d). Parts (a) and (c) display the effect of errors in observed ΔNe, while parts (b) and (d) display the effect of errors in $\Delta N_2/Ar$. Results for different diffusive gas exchange parameterizations and eddy diffusivities (K_z) are shown. The lines were derived by offsetting the gas observations used in the model inversion to determine the effect on bubble fluxes. The gray bars indicate our estimate of the actual errors in ΔNe and $\Delta N_2/Ar$.

almost no effect on the $\Delta N_2/Ar$ of the mixed layer. In contrast, the transfer of Ne by both injection and exchange can increase the ΔNe of the mixed layer. The consequence of this is that our model essentially solves for the injection bubble flux almost exclusively from the $\Delta N_2/Ar$ mass balance. Then, given the injection flux determined from $\Delta N_2/Ar$, the ΔNe mass balance is used to solve for the exchange bubble flux. The result of this is that months with high observed $\Delta N_2/Ar$ ratios have high injection fluxes, while months with high ΔNe but low $\Delta N_2/Ar$ tend to have high exchange fluxes (compare Figs. 4 and 6). This explains why errors in ΔNe do not affect estimates of injection, so that the small error in our $\Delta N_2/Ar$ measurements produces a well-constrained injection flux (Fig. A1). The exchange flux cannot be determined with as much certainty because it is sensitive to errors in both the ΔNe and $\Delta N_2/Ar$ measurements.

Errors in the monthly ΔNe and $\Delta N_2/Ar$ data were large enough that injection and exchange fluxes determined for each time period between cruises were not well constrained. To avoid biases, negative bubble fluxes were not excluded from the annual integrations, even though negative bubble fluxes have no real physical meaning. Including negative bubble fluxes had no impact on estimates of productivity because biological O_2 production was diagnosed from $\Delta O_2/Ar$, which is insensitive to both bubble mechanisms.

The characteristics of our bubble-flux inversion also explain why increasing the eddy diffusivity lowered the flux from the exchange mechanism somewhat but had no effect on the injection flux. $\Delta N_2/Ar$ has almost no gradient with depth in the upper water column, so increased mixing does not affect mixed layer $\Delta N_2/Ar$ or therefore the injection estimate. Neon concentrations do increase slightly with depth, so increased mixing supplies more Ne to the mixed layer, reduces the amount of Ne that must be supplied by bubbles, and results in a lower bubble exchange flux.

REFERENCES

Anderson, L. A. 1995. On the hydrogen and oxygen content of marine phytoplankton. Deep-Sea Res. I, *42*, 1675–1680.

Asher, W. E. and R. Wanninkhof. 1998a. The effect of bubble-mediated gas transfer on purposeful dual-gaseous tracer experiments. J. Geophys. Res., *103*, 10555–10560.

——— 1998b. Transient tracers and air-sea gas transfer. J. Geophys. Res., *103*, 15939–15958.

Baker, K. S. and R. Frouin. 1987. Relation between photosynthetically available radiation and total insolation at the ocean surface under clear skies. Limnol. Oceanogr., *32*, 1370–1377.

Benitez-Nelson, C., K. O. Buesseler, D. M. Karl and J. Andrews. 2001. A time-series study of particulate matter export in the North Pacific Subtropical Gyre based on ^{234}Th:^{238}U disequilibrium. Deep-Sea Res. I, *48*, 2595–2611.

Bingham, F. M. and R. Lukas. 1996. Seasonal cycles of temperature, salinity and dissolved oxygen observed in the Hawaii Ocean time-series. Deep-Sea Res. II, *43*, 199–213.

Bishop, J. K. B., W. B. Rossow and E. G. Dutton. 1997. Surface solar irradiance from the International Satellite Cloud Climatology Project 1983–1991. J. Geophys. Res., *102*, 6883–6910.

Brainerd, K. E. and M. C. Gregg. 1993. Diurnal restratification and turbulence in the oceanic surface mixed layer. 1. Observations. J. Geophys. Res., *98*, 22645–22656.

Chiswell, S. M. 1994. Using an array of inverted echo sounders to measure dynamic height and geostrophic current in the North Pacific subtropical gyre. J. Atmos. Oceanic Tech., *11*, 1420–1424.

Christian, J. 2005. Biogeochemical cycling in the oligotrophic ocean: Redfield and non-Redfield models. Limnol. Oceanogr., *50*, 646–657.

Clark, N. E., L. Eber, R. Laurs, J. A. Renner and J. F. T. Saur. 1974. Heat exchange between ocean and atmosphere in the eastern North Pacific for 1961–71. Tech. Rep., NOAA, U.S. Dept. of Comm., Washington DC.

Craig, H. and T. Hayward. 1987. Oxygen supersaturation in the ocean: Biological versus physical contributions. Science, *235*, 199–202.

da Silva, A. M., C. C. Young and S. Levitus. 1994. Atlas of surface marine data 1994, Vol. 4: Anomalies of fresh water fluxes. NOAA Atlas, NESDIS, 9, NOAA, U.S. Dept. of Comm., Washington, DC, 308 pp.

Davis, R. E., R. deSzoeke, D. Halpern and P. Niller. 1981. Variability in the upper ocean during MILE. Part I: The heat and momentum balances. Deep-Sea Res. A, *28*, 1427–1451.

Doney, S. C. 1996. A synoptic atmospheric surface forcing data set and physical upper ocean model for the U.S. JGOFS Bermuda Atlantic Time-series Study site. J. Geophys. Res., *101*, 25615–25634.

Emerson, S., P. Quay, D. Karl, C. Winn, L. Tupas and M. Landry. 1997. Experimental determination of the organic carbon flux from open-ocean surface waters. Nature, *389*, 951–954.

Emerson, S., P. D. Quay, C. Stump, D. Wilbur and R. Schudlich. 1995. Chemical tracers of productivity and respiration in the subtropical Pacific Ocean. J. Geophys. Res., *100*, 15873–15887.

Emerson, S., C. Stump, B. Johnson and D. M. Karl. 2002. *In situ* determination of oxygen and nitrogen dynamics in the upper ocean. Deep-Sea Res. I, *49*, 941–952.

Emerson, S., C. Stump, D. Wilbur and P. Quay. 1999. Accurate measurement of O_2, N_2, and Ar gases in water and the solubility of N_2. Mar. Chem., *64*, 337–347.

Fairall, C. W., E. F. Bardley, D. P. Rogers, J. B. Edson and G. S. Young. 1996. Bulk parameterization of air-sea fluxes for Tropical Ocean–Global Atmosphere Coupled–Ocean Atmosphere Response Experiment. J. Geophys. Res., *101*, 3747–3764.

Falkowski, P. G., R. T. Barber and V. Smetacek. 1998. Biogeochemical controls and feedbacks on ocean primary production. Science, *281*, 200–206.

Finnigan, T. D., D. S. Luther and R. Lukas. 2002. Observations of enhanced diapycnal mixing near the Hawaiian ridge. J. Phys. Oceanogr., *32*, 2988–3002.

Fuchs, G., W. Roether and P. Schlosser. 1987. Excess ^{3}He in the ocean surface layer. J. Geophys. Res., *92*, 6559–6568.

Fujieki, L. A., F. Santiago-Mandujano, C. Sheridan, R. Lukas and D. Karl. 2004. Hawaii Ocean Time-series data Report 13: 2001. Tech. Rep., University of Hawaii, Honolulu.

García, H. E. and L. I. Gordon. 1992. Oxygen solubility in seawater: Better fitting equations. Limnol. Oceanogr., *37*, 1307–1312.

——— 1993. Erratum: Oxygen solubility in seawater: Better fitting equations. Limnol. Oceanogr., *38*, 656.

Gregg, M. C. 1989. Scaling turbulent dissipation in the thermocline. J. Geophys. Res., *94*, 9686–9698.

——— 1998. Estimation and geography of diapycnal mixing in the stratified ocean, *in* Physical processes in lakes and oceans, J. Imberger, ed., American Geophysical Union, Washington, DC, 305–338.

Hamme, R. C. 2003. Applications of neon, nitrogen, argon and oxygen to physical, chemical and biological cycles in the ocean. Ph.D. thesis, University of Washington, 177 pp.

Hamme, R. C. and S. R. Emerson. 2002. Mechanisms controlling the global oceanic distribution of the inert gases argon, nitrogen and neon. Geophys. Res. Lett., *29*, doi:10.1029/2002GL015273, 2120.

——— 2004a. Measurement of dissolved neon by isotope dilution using a quadrupole mass spectrometer. Mar. Chem., *91*, 53–64.

——— 2004b. The solubility of neon, nitrogen and argon in distilled water and seawater. Deep-Sea Res. I, *51*, 1517–1528.

Jähne, B., K. O. Münnich, R. Bösinger, A. Kutzi, W. Huber and P. Libner. 1987. On the parameters influencing air-water gas exchange. J. Geophys. Res., *92*, 1937–1949.

Jenkins, W. J. 1988. The use of anthropogenic tritium and helium-3 to study subtropical gyre ventilation and circulation. Philos. Trans. R. Soc. Lond., A, *325*, 43–61.

Jenkins, W. J. and J. C. Goldman. 1985. Seasonal oxygen cycling and primary production in the Sargasso Sea. J. Mar. Res., *43*, 465–491.

Josey, S. A., D. Oakley and R. W. Pascal. 1997. On estimating the atmospheric longwave flux at the ocean surface from ship meteorological reports. J. Geophys. Res., *102*, 27961–27972.

Kaiser, J., M. K. Reuer, B. Barnett and M. L. Bender. 2005. Marine productivity estimates from continuous O_2/Ar ratio measurements by membrane inlet mass spectrometry. Geophys. Res. Lett., *32*, doi: 10.1029/200561023459, L19605.

Kalnay, E. and Coauthors. 1996. The NCEP/NCAR 40-year Reanalysis Project. Bull. Amer. Meteor. Soc., *77*, 437–471.

Kantha, L. H. and C. A. Clayson. 1996. An improved mixed layer model for geophyscial applications. J. Geophys. Res., *99*, 25235–25266.

Karl, D. M. and R. Lukas. 1996. The Hawaii Ocean Time-series (HOT) program: Background rationale and field implementation. Deep-Sea Res. II, *43*, 129–156.

Keeling, R. 1993. On the role of large bubbles in air-sea gas exchange and supersaturation in the ocean. J. Mar. Res., *51*, 237–271.

Large, W. G. and G. B. Crawford. 1995. Observations and simulations of upper-ocean response to wind events during the Ocean Storms Experiment. J. Phys. Oceanogr., *25*, 2831–2852.

Large, W. G., J. C. McWilliams and S. C. Doney. 1994. Ocean vertical mixing: A review and a model with a nonlocal boundary layer parameterization. Rev. Geophys., *32*, 363–403.

Laws, E. A., P. G. Falkowski, W. O. Smith, Jr., H. Ducklow and J. J. McCarthy. 2000. Temperature effects on export production in the open ocean. Global Biogeochem. Cycles, *14*, 1231–1246.

Letelier, R. M., D. M. Karl, M. R. Abbott and R. R. Bidigare. 2004. Light driven seasonal patterns of chlorophyll and nitrate in the lower euphotic zone of the North Pacific Subtropical Gyre. Limnol. Oceanogr., *49*, 508–519.

Liss, P. S. and L. Merlivat. 1986. Air-sea gas exchange rates: Introduction and synthesis, *in* The Role of Air-Sea Exchange in Geochemical Cycling, P. Buat-Ménard, ed., D. Reidel, Hingham, MA, 113–127.

McNeil, C. L., B. D. Johnson and D. M. Farmer. 1995. *In-situ* measurement of dissolved nitrogen and oxygen in the ocean. Deep-Sea Res. I, *42*, 819–826.

Memery, L. and L. Merlivat. 1985. Modelling of gas flux through bubbles at the air-water interface. Tellus B, *37*, 272–285.

Mitchum, G. T. 1996. On using satellite altimetric heights to provide a spatial context for the Hawaii Ocean Time-series measurements. Deep-Sea Res. II, *43*, 257–280.

Monahan, E. C. and T. Torgersen. 1991. Enhancement of air-sea gas exchange by oceanic whitecapping, *in* Air-water Mass Transfer: Selected Papers from the Second International Symposium on Gas Transfer at Water Surfaces, S. C. Wilhelms and J. S. Gulliver, eds., American Society of Civil Engineers, New York, NY, 608–617.

Musgrave, D. L., J. Chou and W. J. Jenkins. 1988. Application of a model of upper-ocean physics for studying seasonal cycles of oxygen. J. Geophys. Res., *93*, 15679–15700.

Nightingale, P. D., G. Malin, C. S. Law, A. J. Watson, P. S. Liss, M. I. Liddicoat, J. Boutin and R. C. Upstill-Goddard. 2000. *In situ* evaluation of air-sea gas exchange parameterizations using novel conservative and volatile tracers. Global Biogeochem. Cycles, *14*, 373–387.

Paulson, C. A. and J. J. Simpson. 1977. Irradiance measurements in the upper ocean. J. Phys. Oceanogr., *7*, 952–956.

Payne, R. E. 1972. Albedo of the sea surface. J. Atmos. Sci., *29*, 959–970.

Press, W. H., S. A. Teukolsky, W. T. Vetterling and B. P. Flannery. 1995. Numerical Recipes in C: The Art of Scientific Computing, Cambridge University Press, Cambridge, 2nd ed., 994 pp.

Price, J. F., C. N. K. Mooers and J. C. V. Leer. 1978. Observation and simulation of storm-induced mixed-layer deepening. J. Phys. Oceanogr., *8*, 582–599.

Price, J. F., R. A. Weller and R. Pinkel. 1986. Diurnal cycling: Obervations and models of the upper ocean response to diurnal heating, cooling, and wind mixing. J. Geophys. Res., *91*, 8411–8427.

Quay, P. and J. Stutsman. 2003. Surface layer carbon budget for the subtropical N. Pacific: $\delta^{13}C$ constraints at station ALOHA. Deep-Sea Res. I, *50*, 1045–1061.

Robertson, J. E. and A. J. Watson. 1992. Thermal skin effect of the surface ocean and its implication for CO_2 uptake. Nature, *358*, 738–740.

Roden, G. I. 1980. On the subtropical frontal zone north of Hawaii during winter. J. Phys. Oceanogr., *10*, 342–362.

Schudlich, R. and S. Emerson. 1996. Gas saturation in the surface ocean: The role of heat flux, gas exchange and bubbles. Deep-Sea Res. II, *43*, 569–590.

Seckel, G. R. 1968. A time-sequence oceanography investigation in the North Pacific trade-wind zone. Trans. Am. Geophys. Union, *49*, 377–387.

Shulenberger, E. and J. L. Reid. 1981. The Pacific shallow oxygen maximum, deep chlorophyll maximum, and primary productivity, reconsidered. Deep-Sea Res. A, *28*, 901–919.

Siegenthaler, U. and J. L. Sarmiento. 1993. Atmospheric carbon dioxide and the ocean. Nature, *365*, 119–125.

Smith, S. R., D. M. Leller and K. V. Verzone. 2001. Quantifying uncertainties in NCEP reanalyses using high-quality research vessel observations. J. Climate, *14*, 4062–4072.

Sonnerup, R. E., P. D. Quay and J. L. Bullister. 1999. Thermocline ventilation and oxygen utilization rates in the subtropical North Pacific based on CFC distributions during WOCE. Deep-Sea Res. I, *46*, 777–805.

Spitzer, W. S. and W. J. Jenkins. 1989. Rates of vertical mixing, gas exchange and new production: Estimates from seasonal gas cycles in the upper ocean near Bermuda. J. Mar. Res., *47*, 169–196.

Wanninkhof, R. 1992. Relationship between wind speed and gas exchange over the ocean. J. Geophys. Res., *97*, 7373–7382.

Woolf, D. K. and S. A. Thorpe. 1991. Bubbles and the air-sea exchange of gases in near-saturation conditions. J. Mar. Res., *49*, 435–466.

Received: *18 January, 2005;* revised: *15 November, 2005*.